Research on Farmland Extraction from Remote Sensing Images Based on Decision Tree

Liang Wu[1,*] and LanPing Xiao[2,†]
[1]School of Information and Media, Hubei Land Resources Vocational College Wuhan, Hubei, 430090, China
[2]School of Computer Science, China University of Geosciences, Wuhan, Hubei, 430074, China

Keywords: Decision Tree, Random Forest, Remote Sensing Image, Cropland Information Extraction.

Abstract: In recent years, along with the rapid development of science and technology and the rapid increase of China's population, urbanization has become more and more serious, and the decrease of arable land will directly lead to food crisis and thus social problems, therefore, the statistical monitoring of arable land area is especially important. In this paper, we propose a random forest-based construction of multiple decision tree model to segment and extract remote sensing image plots for research. In this paper, a graph theory-based segmentation method is used for image segmentation, and the Canny edge operator is introduced to extract edge information, which is used to suppress the over-segmentation phenomenon generated by it. Next, it is optimized using a Bagging-based random forest expansion algorithm. We conducted experiments on the hyperspectral remote sensing image number dataset captured by the Resource 3 (ZY-3) satellite provided by MathorCup, and finally obtained an accuracy of 88.09%.

1 INTRODUCTION

In recent years, along with the rapid development of science and technology and the rapid increase of our population, urbanization has become more and more serious, and the decrease of arable land can directly lead to food crisis and thus social problems. Therefore, we investigate this problem from the perspective of image classification.

The first proposed image segmentation algorithms were threshold-based and edge-region-based segmentation methods, and Felzenszwalb and Huttenlocher (Felzenszwalb & Huttenlocher, 2004) proposed an efficient graph-based image segmentation theory in 2004 to achieve the retention of detailed features in regions with a low degree of variability while ignoring height variation and regional detail features. In 2018, Ratna Saha,Mariusz Bajger and Gobert Lee (R. et al., 2018) proposed a study using graph based segmentation approach to segment nucleus from cytology images. In the same year, Cahuina, Edward Cayllahua and his team (Cahuina et al., 2018) propose a series of algorithms to compute the result of the hierarchical graph-based image segmentation method. In 2019, Cahuina, Edward Cayllahua and his team (Cahuina et al., 2019) is devoted to providing a series of algorithms to compute the result of this hierarchical graph-based image segmentation method efficiently. In the same year, Shirly, S and Ramesh, K (Shirly & Ramesh, 2019) provided an insight about different 2-Dimensional and 3-Dimensional MRI image segmentation techniques and summarized the benefits and limitations of various segmentation techniques.

This paper describes the construction method of the model, firstly, after pre-processing the image by filtering and selecting the features, it introduces the optimization of image segmentation by introducing the Canny edge operator, then it introduces the random forest to upgrade the decision tree, and finally the experimental results are obtained after removing the image noise, and the performance of the model on the dataset is analyzed.

Wu, L. and Xiao, L.
Research on Farmland Extraction from Remote Sensing Images Based on Decision Tree.
DOI: 10.5220/0011918000003612
In *Proceedings of the 3rd International Symposium on Automation, Information and Computing (ISAIC 2022)*, pages 209-215
ISBN: 978-989-758-622-4; ISSN: 2975-9463

2 RELATED WORK

2.1 Image Segmentation

2.1.1 Edge Detection

The edge detection mainly consists of five steps, such as grayscale processing, filtering fuzzy, gradient calculation, etc. The specific algorithms are as follows.

(1) Grayscale processing. A color image is converted into a grayscale image by making the R, G, and B components of the color equal.

The grayscale processing in this paper is performed using the weighted average method with the formula shown in equation (1).

$$Gray(i,j) = 0.299 * R(i,j) + 0.578 * G(i,j) + 0.114 * B(i,j) \quad (1)$$

(2) Processing by bilateral filtering method.

(3) Calculating gradient value and direction. Image gradient is the partial derivative of the pixel point currently located for the X and Y axes, and the gradient is the rate of change of the pixel gray value in the image processing field. Defined as the image gray value, assigned to the X-direction gradient, assigned to the Y-direction gradient, assigned to the point, the gradient direction (angle), as shown in equation (2).

$$P(i,j) = (f(i-1,j) - f(i,j) + f(i+1,j+1) - f(i,j+1))/2$$
$$Q(i,j) = (f(i,j) - f(i,j+1) + f(i+1,j) - f(i+1,j+1))/2$$
$$M(i,j) = \sqrt{P(i,j)^2 + Q(i,j)^2}$$
$$\theta(i,j) = \frac{arctan(Q(i,j)}{P(i,j)} \quad (2)$$

(4) Non-maximum suppression. The idea of non-maximal suppression is to search for the local maximum gradient and retain it, and sieve out all other non-maximal values. The specific steps are as follows.

1. Compare the gradient intensity of the current point with the gradient intensity of the points in the positive and negative gradient directions.

2. If the gradient intensity of the current point is the maximum compared to other points in its same direction, then keep it. Otherwise, it is suppressed, i.e. set to 0.

(5) Edge connection. While most of the other conventional algorithms filter out small gradients caused by noise or color changes while maintaining larger gradients by using a threshold, the Canny algorithm uses a double threshold, i.e., a low TL threshold and a high TH threshold to separate edge pixels. According to TL and TH, a point less than TL is set with a 0 marker when connecting the edges of an image; points greater than T H are assigned a value of 1. The 8-connected region is used to define the point between TL and TH, and when a TH pixel point exists in the 8-connected region, it should be designated as a polar point.

2.1.2 Figure Cut Chunking

In the original scheme, it judges whether two regions should be merged based on the inter-region spacing and intra-region spacing. In this paper, based on the extracted edge information, we set the edge weight of adjacent nodes at the edge to infinity to suppress the under-segmentation and over-segmentation phenomena.

Using the satellite image of RBG and the binary image of edge detection as input, the image content is blocked in the following steps.

Let each pixel point of the RGB satellite image be a separate node, and each pixel point is connected with other pixel points in its four-neighborhood range to form $G = (V, E)$, where the edge weights of the edges (v_i, v_j) are their Euclidean distances in the RGB space, as shown in equation (3).

$$w_{vi,vj} = \sqrt{(R_i - R_j)^2 + (G_i - G_j)^2 + (B_i - B_j)^2} \quad (3)$$

Define as the set of edges obtained by edge extraction, introducing edge information to restrict the edge weights when $v_i, v_j \notin edge$ as shown in equation (4), when $v_i | v_j \in edge$, taking ∞ as shown in.

$$w_{v_i,v_j} = \sqrt{\left(R_i - R_j\right)^2 + \left(G_i - G_j\right)^2 + \left(B_i - B_j\right)^2} \quad (4)$$

Define the inter-region spacing as shown in equation (5).

$$Dif(C_1, C_2) = min_{v_i \in C_1, v_j \in C_2, (v_i, v_j) \in E}\, \omega_{v_i,v_j} \quad (5)$$

The intra-definition interval spacing is shown in equation (6).

$$M\,int(C) = max_{e \in MST(C,E)}\, w(e) + \frac{K}{|C|} \quad (6)$$

where *MST* denotes the minimum spanning tree of region *C*, which is defined here as the maximum connected edge length in the region, *k* is a constant, and |*C*| denotes the number of nodes in the region.

The final judgment basis for region merging is obtained by comparing the size relationship between $Dif(C_1, C_2)$and $min(M\,int(C_1), M\,int(C_2))$.

Since the edge detection picture is combined in the construction of the graph structure, for the edge neighbouring points detected in the Canny edge detection in the graph the edge weight is infinite, that

is, the edge information in the edge picture is used as one of the bases for the chunking, so the process of the graph cut chunking can better segment different regions and reduce the phenomenon of incomplete and inappropriate segmentation.

After chunking, the satellite map of farmland can be more complete to divide each object in the image as a whole, after chunking, a piece of farmland in the image is divided out individually, and the subsequent processing takes each area as the processing object. This helps to retain the image characteristics and integrity of the farmland block as a whole. And for different farmland blocks, their colour and other characteristics may be different, and by segmenting each object in the image, it is possible to process different farmland types, forests, houses and other information separately.

2.2 Decision Tree

The decision tree is a tree structure that uses layer by layer inference to achieve classification, and its internal nodes are divided into three categories: one is the root node, which contains the full set of samples; the second is the internal node, which is used to perform feature attribute testing and decide the direction of the next decision; the third is the leaf node, each leaf node contains a definite classification result, and when the attribute test goes to the leaf node means the end of the decision. The main steps of the algorithm are as follows.

(1) Collecting samples.

(2) Select features and construct nodes. According to the importance of features to construct sub-nodes, the more important features are closer to the root node, the more representative genes are selected as features in this problem, the closer genes are to the root node, the importance of genes can be judged by calculating information entropy and Gini coefficient, the formula is shown in equation (7).

$$H(X) = -\sum_{x \in X} p(x) \log p(x) \quad (7)$$

Where *p(x)* represents the probability that a value *x* can be taken. Assuming that there is a sample set *D*, the discrete attribute *a* has *N* possible value $\{a_1, a_2, \ldots a_n\}$, using the partition of the sample set *a*, *N* branching node is created. The *i* branch node contains all the samples *D* in the attribute *a* with entropy values a_i, which is denoted as D^i.

The formula for calculating the Gini coefficient is shown in equation (8).

$$Gain(D) = \sum_{k=1}^{k} p_k(1 - p_k) = 1 - \sum_{k=1}^{k} p_k^2 \quad (8)$$

The Gini coefficient reflects the probability that two samples are randomly selected from the dataset *D* with different labels. The smaller the Gini coefficient, the higher the purity of the dataset *D*.

The Gini coefficient of set *D* under attribute *a* is defined as shown in equation (9).

$$Gain(D, a) = \sum_{i=1}^{N} \frac{|D^i|}{|D|} Gini(D^i) \quad (9)$$

Some value of attribute *a* divides D into two parts D^1 and D^2, at which point the Gini coefficient is shown in equation (10).

$$Gain(D, a) = \frac{|D^1|}{|D|} Dini(D^1) + \frac{|D^2|}{|D|} Dini(D^2) \quad (10)$$

(3) Split nodes. Divide the dataset according to the way the features are split, i.e., differentiate according to the conditions.

3 THE IMPROVEMENT

3.1 Random Forest

A random forest is a classifier consisting of multiple unrelated decision trees. When performing a classification task, each time a new sample is input, each decision tree in the forest is allowed to classify and get multiple identical or different results, using voting to get the final forest classification result. Its integrated method implementation based on Bagging makes the accuracy of decision trees rise another big step. The basic steps of its algorithm are as follows.

(1) Divide the training set into n subsets, using m to represent the total number of features.

(2) Input the number of features m, which is used to determine the decision outcome of a node on the decision tree; where m should be much smaller than n.

(3) Create a training set and predict non-negative example errors by sampling n times from the n subsets in a way that has put-back sampling to evaluate the error.

(4) For each node arbitrarily choose m features and calculate its optimal split based on these m features.

(5) Make each tree grow fully instead of pruning branches.

(6) Classify the new data using a random forest classifier composed of the generated multiple decision trees, and decide the classification result according to how many votes the tree classifier has.

The flowchart of the algorithm is shown in Figure 1.

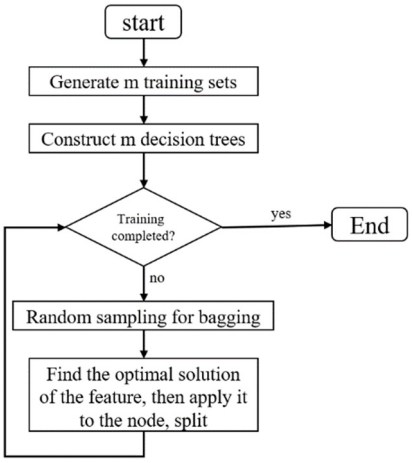

Figure 1: Random forest model flowchart

3.2 Output Image Denoising

Due to the introduction of the Canny edge operator, less edge information is retained in the resultant image. The image is processed using the image erosion expansion operation and the open-close operation, which can effectively remove the redundant edge information while retaining the original shape of the image, with good suppression of edge noise and improved accuracy.

Erosion operation takes the smallest value in the rectangular neighborhood of each position as the output gray value of that position and reduces the gray value, so that the area of bright areas in the image will become smaller and the area of dark areas will increase.

In contrast to erosion, the expansion operation expands the brighter part of the image by finding the local maximum, so that this part has a larger area in the effect image compared with the original image, i.e. the brighter objects in the image will be larger in size and the darker objects will be smaller in size.

The open operation eliminates the small brighter areas in the image by first eroding and then expanding, while the closed operation removes the small black voids in the image by first expanding and then eroding. Both algorithms do not change the area of other objects.

4 EXPERIMENTS PROCESS AND RESLUT ANALYSIS

4.1 Data Sets

The dataset used in this experiment is from the MathorCup Collegiate Mathematical Modeling Challenge. The images were obtained from remote sensing image data acquired by the Resource 3 satellite, China's first autonomous civilian high-resolution stereo mapping satellite, with a spatial resolution of 2 m and a spectrum in the visible band (red, green, and blue). This dataset contains a total of ten hyperspectral remote sensing images, and includes labels (labels) labeled by professionals for cultivated land. In this experiment, we divide the dataset according to the ratio of 4:1, with the first 80% as the training set and 20% as the validation set. An example of the dataset is shown in Figure 2, with the tif image visualized on the left, the label map on the right, and the cultivated land in black.

Figure 2: Example data set

4.2 Evaluation Indicators

For a single figure, the evaluation method is to use the model to predict the labeled figure and compare it with the standard labeled figure, and calculate the accuracy based on the number of pixels and the difference in pixel values between the two figures, as shown in equation (11).

$$\text{Accuracy} = \frac{\sum(RGB_p \text{ equals to } RGB_q)}{N} \quad (11)$$

where N represents the number of pixels, RGB_p and RGB_q represent the pixel values of the pixels in the predicted label map and the standard label map, respectively. For the entire model, the accuracy is the average of the accuracy rates of all images.

4.3 Experiments and Result Analysis

Using the models constructed above for training and prediction, the results of decision trees and random

forests were obtained as shown in Table 1 and Table 2, respectively.

Table 1: Decision tree prediction results and accuracy

Test	Number of zones	Area of arable land(m^2)	Accuracy
Data1.tif	1162	246150	88.06%
Data2.tif	935	263640	91.48%
Data3.tif	1371	217080	78.47%
Data4.tif	1153	226560	85.48%
Data5.tif	1112	187110	82.56%
Data6.tif	873	248580	88.81%
Data7.tif	1158	202680	88.93%
Data8.tif	945	254400	87.42%
Test1.tif	1057	203760	\
Test2.tif	984	260490	\
Average accuracy 86.40%			

Table 2: Random forest prediction results and accuracy

Test	Number of zones	Area of arable land(m^2)	Accuracy
Data1.tif	1162	245700	88.71%
Data2.tif	935	262980	91.66%
Data3.tif	1371	200490	81.50%
Data4.tif	1153	224610	87.48%
Data5.tif	1112	191610	83.45%
Data6.tif	873	247620	89.80%
Data7.tif	1158	190950	88.08%
Data8.tif	945	252750	94.05%
Test1.tif	1057	255240	\
Test2.tif	984	259320	\
Average accuracy 88.09%			

By observing the data in Table 1 and Table 2, it can be seen that the random forest performs better than the decision tree on all eight images of the dataset, with an overall accuracy improvement of 2%, and the model optimization can be considered effective.

The edge detection results, image segmentation results and the final predicted label map part of the images during the experiment are shown in Figure 3,4 and 5.

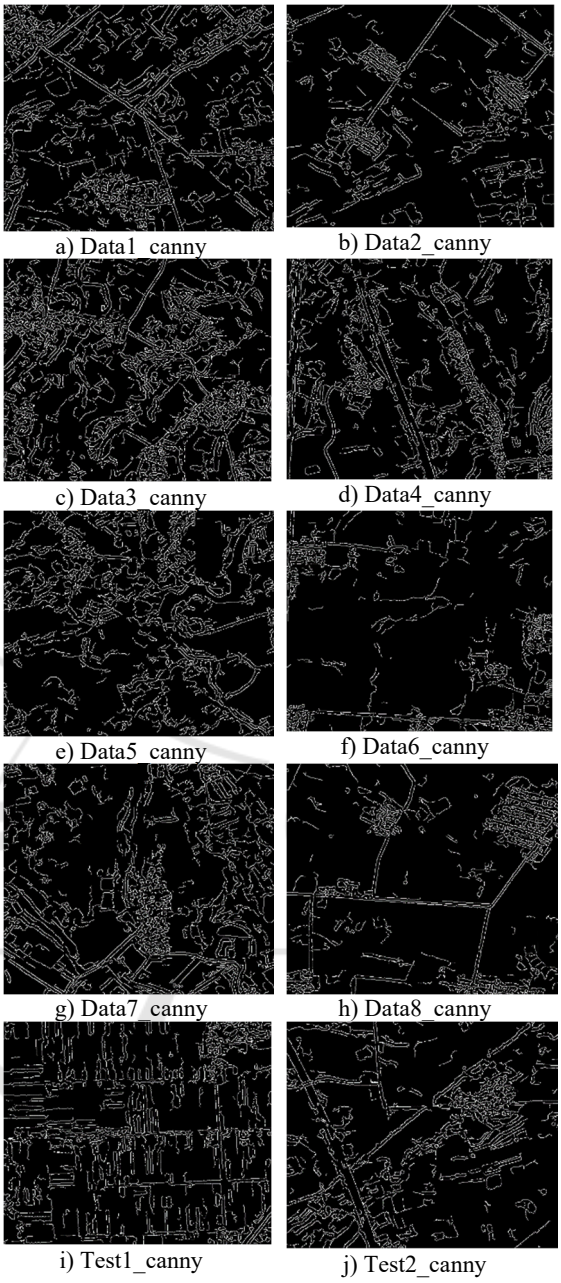

a) Data1_canny b) Data2_canny c) Data3_canny d) Data4_canny e) Data5_canny f) Data6_canny g) Data7_canny h) Data8_canny i) Test1_canny j) Test2_canny

Figure 3: Edge detection results

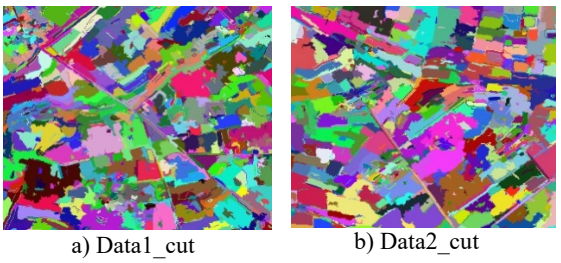

a) Data1_cut b) Data2_cut

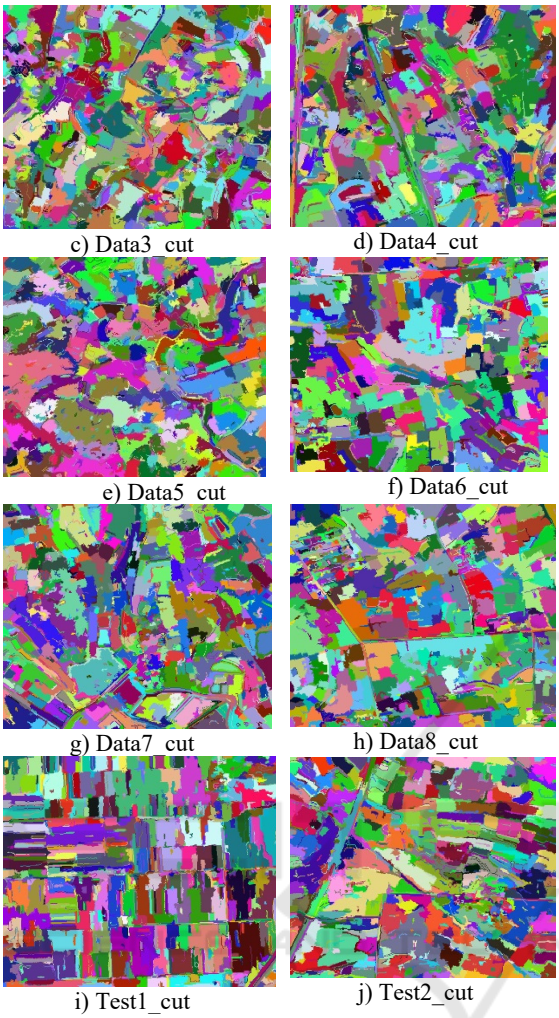

Figure 4: Image segmentation results

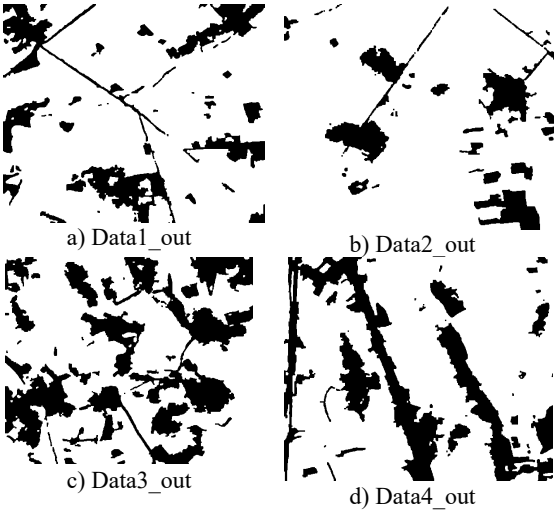

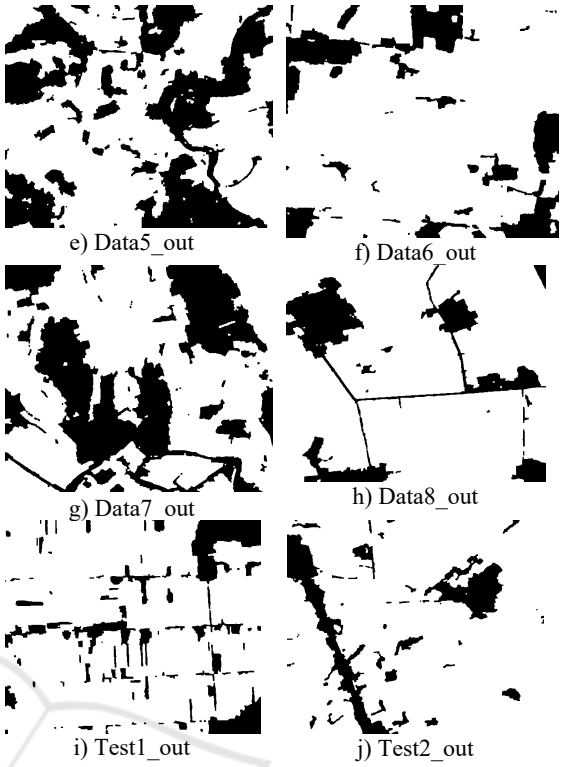

Figure 5: Model prediction results

It is easy to see that the random forest prediction results are much better than the decision tree, and the results are very much as expected, the image segmentation results are good, and the accuracy of the labeled map is close to 90%, so the training can be considered valid.

5 CONCLUSION

In this paper, we proposed a random forest-based construction of multiple decision tree model to segment and extract remote sensing image parcels for research. Firstly, a graph theory-based segmentation method is used for image segmentation, and the Canny edge operator is introduced to extract edge information, which is used to suppress the over-segmentation phenomenon generated by it. Secondly, it is optimized using the Bagging-based random forest expansion algorithm. The accuracy of 88.09% was obtained after conducting the experiment, which gained an improvement compared with the traditional method.

However, our method is not able to completely distinguish all cultivated and non-cultivated land for a single color feature, and the selected features are only selected based on the obvious differences

between cultivated land and other plots that are easily recognized by the naked eye, without considering all features, and the effect of dividing the two regions with inconspicuous edges is not good enough, and for the effect of dividing the region for edge detection, the improved Canny operator or other For the overfitting phenomenon, the overfitting can be reduced by collecting more data sets to train the built model, and if more rich remote sensing images are available, the non-cultivated land can be further divided into multi-classification problems to improve the accuracy of the model for cultivated land recognition.

REFERENCES

Felzenszwalb, P. F., & Huttenlocher, D. P. (2004). Efficient Graph-Based Image Segmentation. *INTERNATIONAL JOURNAL OF COMPUTER VISION*, 59(2), 167-181.

R., S., M., B., & G., L. (2018, 2018-01-01). *Circular Shape Prior in Efficient Graph Based Image Segmentation to Segment Nucleus*. Paper presented at the 2018 Digital Image Computing: Techniques and Applications (DICTA).

Cahuina, E. C., Cousty, J., Kenmochi, Y., Araujo, A. D., Camara-Chavez, G., & CENPARMI. (2018). Algorithms for hierarchical segmentation based on the Felzenszwalb-Huttenlocher dissimilarity *PROCEEDINGS OF THE INTERNATIONAL CONFERENCE ON PATTERN RECOGNITION AND ARTIFICIAL INTELLIGENCE (ICPRAI 2018)* (108-113). International Conference on Pattern Recognition and Artificial Intelligence (ICPRAI).

Cahuina, E. C., Cousty, J., Kenmochi, Y., Araujo, A. D., Camara-Chavez, G., & Guimaraes, S. (2019). Efficient Algorithms for Hierarchical Graph-Based Segmentation Relying on the Felzenszwalb-Huttenlocher Dissimilarity. *INTERNATIONAL JOURNAL OF PATTERN RECOGNITION AND ARTIFICIAL INTELLIGENCE*, 33(11)

Shirly, S., & Ramesh, K. (2019). Review on 2D and 3D MRI Image Segmentation Techniques. *CURRENT MEDICAL IMAGING REVIEWS*, 15(2), 150-160.

Liu, J., Yan, S., Lu, N., Yang, D., Lv, H., Wang, S., Zhu, X., Zhao, Y., Wang, Y., Ma, Z., & Yu, Y. (2022). Automated retinal boundary segmentation of optical coherence tomography images using an improved Canny operator. *Scientific Reports*, 12(1), 1412. http

Singh, S., Tiwari, R. K., Sood, V., Gusain, H. S., & Prashar, S. (2021). Image Fusion of Ku-Band-Based SCATSAT-1 and MODIS Data for Cloud-Free Change Detection Over Western Himalayas. *IEEE transactions on geoscience and remote sensing*, *60*, 1-14.

Moshkov, M. (2022). On the depth of decision trees with hypotheses. *Entropy*, *24*(1), 116.

Wang, F., Wang, Y., Ji, X., & Wang, Z. (2022). Effective Macrosomia Prediction Using Random Forest Algorithm. *International Journal of Environmental Research and Public Health*, *19*(6), 3245.